Supplementary Information for
"Engineering synthetic magnetic fields for polarized photons"

Guohua Liu[1,2,†], Zepei Zeng[1,2,†], Haolin Lin[1,2], Xin Zhang[1,2], Xiliang Zhang[1,2],
Yanwen Hu[1,2,3], Zhen Li[1,2,3*], Zhenqiang Chen[1,2,3], and Shenhe Fu[1,2,3*]

[1]*Department of Optoelectronic Engineering, Jinan University, Guangzhou 510632, China*

[2]*Guangdong Provincial Key Laboratory of Optical Fiber Sensing and Communications, Guangzhou 510632, China*

[3]*Guangdong Provincial Engineering Research Center of Crystal and Laser Technology, Guangzhou 510632, China*

Section A: Theoretical model for the synthetic two-level system

We identify an effective photonic two-level system, where two orthogonally polarized photon states define the pseudo spin up and spin down. We examine coherent couplings between these two pseudo spins in an engineered anisotropic medium. To address this problem, we start from the Maxwell equation

$$\nabla \times [\mu^{-1} \cdot (\nabla \times \tilde{\mathbf{E}})] = -\hat{\epsilon} \cdot \frac{\partial^2 \tilde{\mathbf{E}}}{\partial t^2}, \tag{S1}$$

where $\tilde{\mathbf{E}}$ denotes the electromagnetic field, μ and $\hat{\epsilon}(x, y)$ are the permeability and dielectric tensor of the anisotropic medium. t is the elapsed time. Considering a harmonic wave form: $\tilde{\mathbf{E}} = \mathbf{E}(x, y, z)\exp(-i\omega t)$, where ω is the carrier frequency, the linearly coupled-wave equation defined in the cartesian coordinate system is derived as

$$\begin{aligned} \nabla^2 E_x + \beta_x^2 E_x &= \frac{\partial}{\partial x}(\nabla \cdot \mathbf{E}), \\ \nabla^2 E_y + \beta_y^2 E_y &= \frac{\partial}{\partial y}(\nabla \cdot \mathbf{E}), \\ \nabla^2 E_z + \beta_z^2 E_z &= \frac{\partial}{\partial z}(\nabla \cdot \mathbf{E}), \end{aligned} \tag{S2}$$

where $\beta_j = \omega\sqrt{\mu\epsilon_j}$ $(j = x, y, z)$ represents a propagation constant of the corresponding wave component E_j in the medium. When the dielectric medium is isotropic, we have $\nabla \cdot \mathbf{E} = 0$. As a result, the three components become decoupled and propagate independently through the medium. However, the anisotropic medium couples the different wave components during propagation, leading to photonic spin-orbit couplings. We point out that the electromagnetic field satisfies the relationship: $\epsilon_x \partial E_x/\partial x + \epsilon_y \partial E_y/\partial y + \epsilon_z \partial E_z/\partial z = 0$. We consider an approximation of the slowly varying envelope along with z, namely $\partial^2 E_x/\partial z^2 \ll \beta_x \partial E_x/\partial z$ and $\partial^2 E_y/\partial z^2 \ll \beta_y \partial E_y/\partial z$. With these conditions, we reduce the coupled-wave equation to a simpler two-component form, written as

$$\begin{aligned} 2i\beta_x \frac{\partial E_x}{\partial z} + \frac{\epsilon_x}{\epsilon_z}\frac{\partial^2 E_x}{\partial x^2} + \frac{\partial^2 E_x}{\partial y^2} &= \gamma_y \frac{\partial^2 E_y}{\partial y \partial x}\exp(+i\Delta\beta \cdot z), \\ 2i\beta_y \frac{\partial E_y}{\partial z} + \frac{\epsilon_y}{\epsilon_z}\frac{\partial^2 E_y}{\partial y^2} + \frac{\partial^2 E_y}{\partial x^2} &= \gamma_x \frac{\partial^2 E_x}{\partial x \partial y}\exp(-i\Delta\beta \cdot z). \end{aligned} \tag{S3}$$

Here $\gamma_j = 1 - \epsilon_j/\epsilon_z$ denotes an inhomogeneous anisotropic coefficient of the medium, which couples these two polarization components (two pseudo spins: E_x and E_y). We define a position-dependent phase mismatch quantity as $\Delta\beta(x, y) = \beta_y - \beta_x$, which is originating from mutual beating between the two pseudo spins during evolution in the medium. In the following, we consider using a transformation of the two-component coupled-wave equation to the rotating frame, by defining

$$E_x = A_x \exp(+i\Delta\beta \cdot z/2),$$
$$E_y = A_y \exp(-i\Delta\beta \cdot z/2). \tag{S4}$$

In the rotating frame, the coupled-wave equation is modified as

$$i\frac{\partial A_x}{\partial z} + \frac{1}{2\beta_x}(\nabla_T^2 A_x - \gamma_x \frac{\partial^2 A_x}{\partial x^2}) - \frac{\Delta\beta}{2}A_x = \frac{\gamma_y}{2\beta_x}\frac{\partial^2 A_y}{\partial y \partial x},$$
$$i\frac{\partial A_y}{\partial z} + \frac{1}{2\beta_y}(\nabla_T^2 A_y - \gamma_y \frac{\partial^2 A_y}{\partial y^2}) + \frac{\Delta\beta}{2}A_y = \frac{\gamma_x}{2\beta_y}\frac{\partial^2 A_x}{\partial x \partial y}, \tag{S5}$$

where $\nabla_T^2 = \partial_x^2 + \partial_y^2$ is a transverse momentum operator. Note that we have assumed that $\bar{\beta} \approx (\beta_x + \beta_y)/2$ and $\bar{\gamma} \approx (\gamma_x + \gamma_y)/2$, by considering the shallow linear birefringence of the photonic structure. In this case, we have $\left|\bar{\gamma}\frac{\partial^2 A_x}{\partial x^2}\right| \ll \left|\nabla_T^2 A_x\right|$ and $\left|\bar{\gamma}\frac{\partial^2 A_y}{\partial y^2}\right| \ll \left|\nabla_T^2 A_y\right|$. Within these conditions, we obtain a magnetic-like Hamiltonian, governing the propagation dynamics of photons in the rotating frame. The corresponding Schrödinger-like equation for the polarized photon state (pseudo spinor) $A = (A_x, A_y)^{\mathrm{T}}$ is then expressed as

$$i\frac{\partial}{\partial z}\begin{pmatrix} A_x \\ A_y \end{pmatrix} = \begin{pmatrix} -\nabla_T^2/(2\bar{\beta}) + \Delta\beta/2 & \bar{\gamma}\nabla_{yx}/(2\bar{\beta}) \\ \bar{\gamma}\nabla_{xy}/(2\bar{\beta}) & -\nabla_T^2/(2\bar{\beta}) - \Delta\beta/2 \end{pmatrix}\begin{pmatrix} A_x \\ A_y \end{pmatrix}, \tag{S6}$$

where $\nabla_{yx} = \partial^2/(\partial y \partial x)$ and $\nabla_{xy} = \partial^2/(\partial x \partial y)$ (they have property $\nabla_{xy} = \nabla_{yx}$). The Hamiltonian governs motions of the spinor in the synthetic two-level system. Accordingly, the equivalent Pauli equation for the two-level photons is written as

$$i\frac{\partial}{\partial z}\begin{pmatrix} A_x \\ A_y \end{pmatrix} = \left(\frac{\boldsymbol{p}_T^2}{2M} - \mu_S \boldsymbol{\sigma} \cdot \mathbf{B}_S\right)\begin{pmatrix} A_x \\ A_y \end{pmatrix}, \tag{S7}$$

where $\boldsymbol{p}_T^2 = [-\nabla_T^2, 0; 0, -\nabla_T^2]$ is a square matrix, denoting a transverse momentum operator. $M = \bar{\beta}$ represents an equivalent mass of the pseudo spinor $\mathbf{A} = (A_x, A_y)^T$, and μ_S is the synthetic magnetic moment of photon, with its value being $\mu_S = 1$. $\boldsymbol{\sigma}$ denotes the Pauli matrix vector. The resulting synthetic magnetic field is obtained as

$$\mathbf{B}_S(x, y) = -\hat{x}\frac{\bar{\gamma}\nabla_{yx}}{2\bar{\beta}} - \hat{z}\frac{\Delta\beta(x, y)}{2}. \tag{S8}$$

Clearly, equation (S7) shows a mathematical equivalent to equation (1) (see the main text) for a massive spinning particle being evolution in time. The obtained synthetic magnetic field presented in Eq. (S8) allows us to effectively manipulate the synthetic magnetic moments of the polarized photons, leading to intriguing spin transport phenomena as demonstrated in the main text.

Section B: Initial pseudo spin preparation

B1: Pseudo spin with homogeneous spin vector

In this subsection, we consider using a half wave plate (HWP) to manipulate the initial pseudo spins of photons which exhibit homogeneous spin vectors. In the experiments, the He-Ne laser is linearly polarized, with its normalized polarization state denoted as $\mathbf{A}_{\text{in}} = (\cos\xi, \sin\xi)^{\text{T}}$, where ξ represents a polarization angle with respect to the x axis. For simplicity, we let the He-Ne laser linearly polarized along x coordinate, in which case the incident pseudo spin is written as

$$\mathbf{A}_{\text{in}} = \begin{pmatrix} 1 \\ 0 \end{pmatrix}. \tag{S9}$$

We note that the Jones matrix of the HWP can be written as follow:

$$\mathbf{J}_{\text{HWP}} = \begin{pmatrix} \cos(2\alpha_1) & \sin(2\alpha_1) \\ \sin(2\alpha_1) & -\cos(2\alpha_1) \end{pmatrix}, \tag{S10}$$

where α_1 is a position-independent angle between the fast axis of the HWP and the horizontal (x) axis. The polarized photon state after passing through the HWP can be represented as:

$$\mathbf{A} = \mathbf{J}_{\text{HWP}} \cdot \mathbf{A}_{\text{in}} = \begin{pmatrix} \cos(2\alpha_1) & \sin(2\alpha_1) \\ \sin(2\alpha_1) & -\cos(2\alpha_1) \end{pmatrix} \begin{pmatrix} 1 \\ 0 \end{pmatrix} = \begin{pmatrix} \cos(2\alpha_1) \\ \sin(2\alpha_1) \end{pmatrix}. \tag{S11}$$

It is evident that the pseudo spin of photons can be customized by simply rotating the HWP (namely tuning the angle α_1). Different pseudo spins including the purely spin up and spin down, as well as the equally mixing spins, are illustrated in Fig. 2 of the main text. More complex homogeneous pseudo spin can be constructed by further considering a quater wave plate (QWP), as detailed below. It converts the linearly polarized photons into the circularly polarized ones. In the presence of the pseudo spin framework, the spin distributions for these circularly polarized photons are illustrated in Fig. 2 of the main text.

B2: Pseudo spin with inhomogeneous spin vectors

Theoretically, the inhomogeneous pseudo spins are built by a coherent mixing between two orthogonal circular polarization basis with opposite helical wavefronts. The resulting spin exhibits an inhomogeneous distribution of the spin vectors. This can be realized experimentally by using a standard vortex wave plate (VWP) with a consistent delay phase: π. Such an element exhibits a space-varying optical axis, featured by a position-dependent orientation angle (with respect to x coordinate) given by $\alpha_2 = \ell\varphi/2 + \alpha_0$, where ℓ represents a topological number of the VWP, φ denotes an azimuthal angle defined as $\varphi = \arctan(y/x)$, and α_0 being a relatively initial angle that can be precisely controlled by rotating the VWP with respect to the x axis. Considering the delay phase being π (a role of the half wave plate), the Jones matrix of the VWP element can be written as:

$$\mathbf{J}_{\text{VWP}} = \begin{pmatrix} \cos(2\alpha_2) & \sin(2\alpha_2) \\ \sin(2\alpha_2) & -\cos(2\alpha_2) \end{pmatrix}. \tag{S12}$$

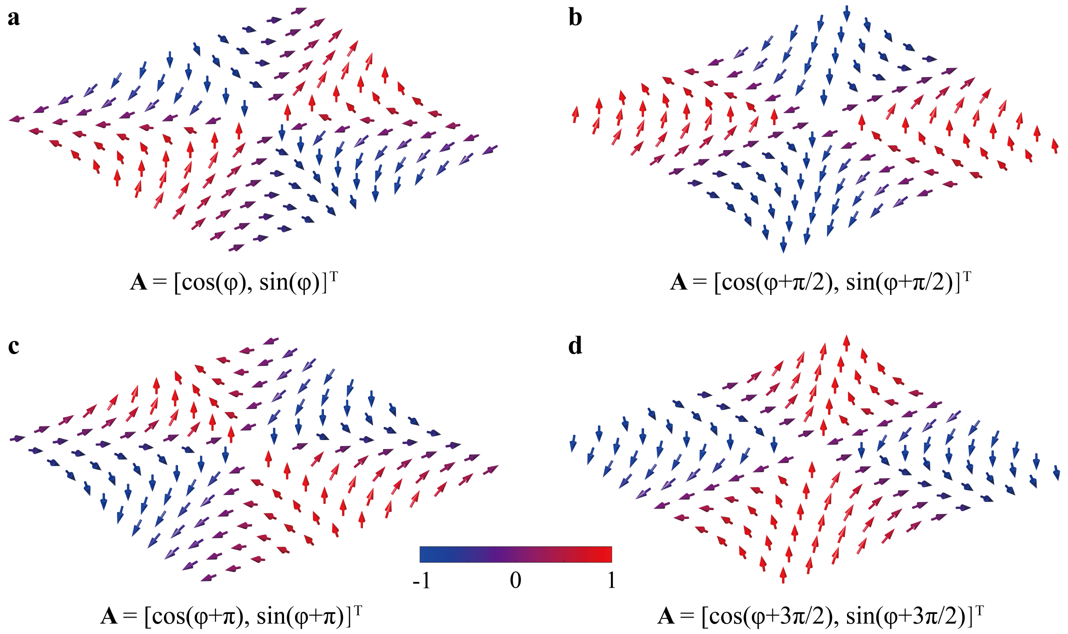

FIG. S1: **Illustrations of the higher-order topological spin structures.** These nontrivial topological spin structures can be realized by using the VWP, which exhibits a space-varying optical axis. As an illustration, we consider the VWP with a topological number being $\ell = 1$. The resulting spin structures are presented, with different settings: **a**, $2\alpha_0 = 0$, **b**, $2\alpha_0 = \pi/2$, **c**, $2\alpha_0 = \pi$, and **d**, $2\alpha_0 = 3\pi/2$.

The VWP is normally illuminated by the laser. The output photon state is expressed as

$$\mathbf{A} = \mathbf{J}_{\text{VWP}} \cdot \mathbf{A}_{\text{in}} = \begin{pmatrix} \cos(2\alpha_2) & \sin(2\alpha_2) \\ \sin(2\alpha_2) & -\cos(2\alpha_2) \end{pmatrix} \begin{pmatrix} 1 \\ 0 \end{pmatrix} = \begin{pmatrix} \cos(2\alpha_2) \\ \sin(2\alpha_2) \end{pmatrix} = \begin{pmatrix} \cos(\ell\varphi + 2\alpha_0) \\ \sin(\ell\varphi + 2\alpha_0) \end{pmatrix}. \tag{S13}$$

The obtained output spin is characterized by the nontrivial topological number ℓ. As a result, the spin vector is space-dependent, with a nontrivial topological structure determined by the order ℓ. Figure S1 illustrates different spin structures with topological charge of $\ell = 1$, by setting $2\alpha_0 = 0$, $2\alpha_0 = \pi/2$, $2\alpha_0 = \pi$, and $2\alpha_0 = 3\pi/2$, see panels **a-d**, respectively. Geometrically, we introduce the higher-order Poincaré sphere to represent the topological spin structures, by setting $\phi = 2\alpha_0$, see Fig. 6**a** in the main text. In this case, the parameter ϕ denotes an azimuthal angle along the equator of the sphere. The output photon state shown in Eq. (S13) can be therefore mapped onto the equator of the higher-order Poincaré sphere with a topological charge of ℓ.

B3: Vortexed pseudo spins

To generate the vortexed pseudo spins, a quater wave plate is inserted between the VWP and HWP elements, see the experimental setup in Fig. 1**d** in the main text. Mathematically, the Jones matrix of the QWP is written as

$$\mathbf{J}_{\text{QWP}} = \frac{\sqrt{2}}{2} \begin{pmatrix} 1 - i\cos(2\alpha_3) & -i\sin(2\alpha_3) \\ -i\sin(2\alpha_3) & 1 + i\cos(2\alpha_3) \end{pmatrix}, \tag{S14}$$

where α_3 is a position-independent angle between the fast axis of the QWP and the x axis, similar to the definition of α_1 for the HWP. The QWP element is able to convert the linearly polarized photons from the laser into the circularly polarized ones, provided that α_3 is set to $\pm 45^{\text{o}}$. In this scenario, the right- and left-handed circularly polarized photons emerging from the QWP can be expressed as: $\mathbf{A}_{\text{R}} = \mathbf{J}_{\text{QWP}}^{45^\circ} \cdot \mathbf{A}_{\text{in}} = \sqrt{2}/2[1, -i]^{\text{T}}$ and $\mathbf{A}_{\text{L}} = \mathbf{J}_{\text{QWP}}^{-45^\circ} \cdot \mathbf{A}_{\text{in}} = \sqrt{2}/2[1, i]^{\text{T}}$, respectively. In the following, we consider using the VWP to transform the circularly polarized photons into the vortexed ones. The corresponding output states take the following forms:

$$\mathbf{A} = \mathbf{J}_{\text{VWP}} \cdot \mathbf{A}_{\text{L}} = \frac{\sqrt{2}}{2} \begin{pmatrix} \cos(2\alpha_2) & \sin(2\alpha_2) \\ \sin(2\alpha_2) & -\cos(2\alpha_2) \end{pmatrix} \begin{pmatrix} 1 \\ i \end{pmatrix} = \frac{\sqrt{2}}{2} \begin{pmatrix} 1 \\ -i \end{pmatrix} e^{+i2\alpha_2} = \mathbf{A}_{\text{R}} \cdot e^{+i(\ell\varphi + 2\alpha_0)}, \tag{S15}$$

and

$$\mathbf{A} = \mathbf{J}_{\text{VWP}} \cdot \mathbf{A}_{\text{R}} = \frac{\sqrt{2}}{2} \begin{pmatrix} \cos(2\alpha_2) & \sin(2\alpha_2) \\ \sin(2\alpha_2) & -\cos(2\alpha_2) \end{pmatrix} \begin{pmatrix} 1 \\ -i \end{pmatrix} = \frac{\sqrt{2}}{2} \begin{pmatrix} 1 \\ i \end{pmatrix} e^{-i2\alpha_2} = \mathbf{A}_{\text{L}} \cdot e^{-i(\ell\varphi + 2\alpha_0)}. \tag{S16}$$

Clearly, the emerging photons from a combined element (QWP plus VWP) can be regarded as a 'two-level' vortexed spinor, which exhibits a topological structure in the wavefront. The structure can be featured by the topological charge of ℓ or $-\ell$, depending on the right or left handedness.

Section C: Relation between the Stern-Gerlach splitting and synthetic magnetic field strength

In this section, we choose to electrically engineer the phase mismatch profile, synthesizing the space-varying magnetization vector field for the photons. As a result, the obtained synthetic Stern-Gerlach magnetic field is closely related to the applied voltage acting on the medium. We investigate the Stern-Gerlach splitting of a two-polarization mixing pseudo spin, written as $\mathbf{A} = A(r)(1/\sqrt{2}; 1/\sqrt{2})$. In the presence of the magnetic field gradient, the two-polarization spin is gradually splitting into two coherent accelerating paths during propagation in the medium (as shown in Fig. 3 of the main text). Using the experimental setup shown in the main text, we measure the splitting distance at the output face of the medium, with recorded outcomes depicted in Fig. S2. It is shown that the splitting distance is linearly proportional to the applied voltage. The splitting distance increases from 0 mm to 0.24 mm, when the voltage is linearly changed from U=0 to 800 V. This linear relationship is in accordance with those Stern-Gerlach experiments obtained in the quantum mechanism and quantum optics. Our simulations performed based on equation (4) in the main text further confirm this linear relation.

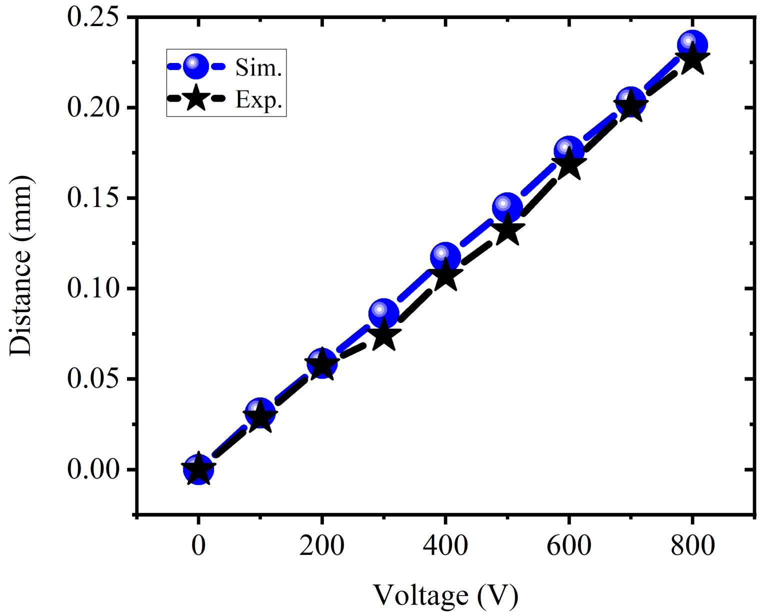

FIG. S2: **The Stern-Gerlach splitting of a mixing pseudo spin, as a function of the applied voltage.** The blue data points denote calculated results based on the equation (4) in the main text; while the black data points indicate the experimental results. The experimental conditions are kept the same with those in Fig. 3 of the main text.

Section D: The Stern-Gerlach effect by using a nondiffracting Bessel envelope

We verify that the demonstrated Stern-Gerlach phenomenon is unaffected by spatial mode profile (gradient) of the carrier, despite the fact that the synthetic magnetic field is associated with spatial gradient of light, see equation (5) in the main text. To verify the assertion, we introduce a formula $\Omega(r_0) = \iint |\nabla_{xy} A(x,y)| dxdy / \iint |A(x,y)| dxdy$ to quantitatively characterize strength of the spatial variation and examine its influence on the Stern-Gerlach effect. To eliminate effect of optical diffraction, we consider a nondiffracting Bessel beam as envelope carrier, the corresponding spinor wave function expressed as $\mathbf{A}(r) = J_0(r/r_0)(1/\sqrt{2}; 1/\sqrt{2})$, where J_0 denotes the zero-order Bessel function and r_0 features the Bessel beam width. We point out that the Bessel beam contains infinite energy, therefore, in practice an exponential function $\exp(-\eta r/r_0)$, where η denotes a decaying factor and is set as $\eta = 0.06$, is utilized to appropriately truncate the ideal Bessel beam. Different cases of $r_0 = 10$ μm, $r_0 = 15$ μm, and $r_0 = 20$ μm are considered, resulting in corresponding gradient strengths: $\Omega = 3.5 \times 10^{-3}$ μm^{-2}, $\Omega = 1.6 \times 10^{-3}$ μm^{-2} and $\Omega = 0.9 \times 10^{-3}$ μm^{-2}, respectively. Clearly, the gradient strength is decreasing with an increasing of r_0. However, our simulations reveal that the variation of spatial gradient of light does not alter the separation distance between the splitted pesudo spin components, as shown in Fig. S3 (**a-c**). This is due to the fact that the cylindrical distribution of light does not induce additional asymmetric force to the photons. This in turn verifies the validity of equation (6) for the 'Lorentz' force. Moreover, Fig. S3 (**a-c**) show that the separated beams are accelerating along parabolic trajectories, while maintaining their Bessel structures [Fig. S3 (**d-f**)]. The Stern-Gerlach effect allows us to achieve nonspreading and accelerating Bessel beams, different from conventional ones that propagate without acceleration.

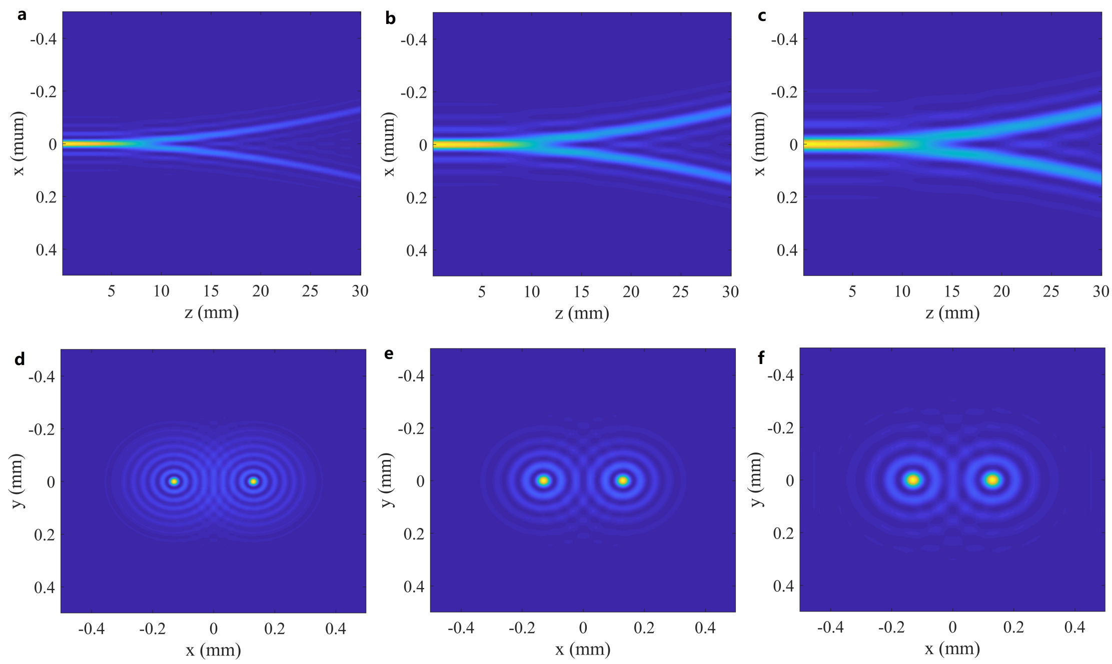

FIG. S3: **The Stern-Gerlach effect obtained by using the nondiffracting Bessel envelope**. Different envelope widths are considered: **a**, $r_0 = 10$ μm; **b**, $r_0 = 15$ μm; **c**, $r_0 = 20$ μm. **a-c**, Photon distributions in the $x-z$ plane, showing that the variation of spatial gradient of envelope does not alter the Stern-Gerlach effect. **d-f**, The corresponding splitted pseudo spin up and spin down components distributed in the $x-y$ plane. These results are obtained with an applied voltage of $U = 600$ V.

Section E: The higher-order Stern-Gerlach effect for the off-equator spin textures

In this section, we study other intriguing higher-order Stern-Gerlach effects by considering the other spin textures mapped on the off-equator of the first-order ($\ell = 1$) Poincaré sphere (Fig. S4**a**). We examine four different spin textures located at (χ, ϕ)= ($\pi/4$, 0), (χ, ϕ)= ($\pi/4$, $\pi/2$), (χ, ϕ)= ($\pi/4$, π) and (χ, ϕ)= ($\pi/4$, $3\pi/2$) on the sphere, respectively. The corresponding spin vector distributions of the higher-order spinors are shown in Fig. S4**a**. These spin textures are different from the on-equator cases as shown in Fig. 6 (the main text), due to the fact that the off-equator spin textures are built by an inhomogeneous elliptical polarization. As a result, we observe a screw distribution of the spin vectors at the center rather than the edge distribution of the on-equator spin vectors. We examine the Stern-Gerlach effect using the same conditions with those in the on-equator cases. Without the synthetic magnetic field gradient ($U = 0$ V), the higher-order spinor propagates along the optical axis without splittings (results not shown here). When the voltage is increased to $U = 600$ V, the induced synthetic magnetic field gradient splits the two orthogonal pesudo spin components from the composite spin textures, see results in Fig. S4**b**-S4**e**. The separated pesudo spins are carried by the Hermite-Gaussian-like envelope rather than the original Laguerre-Gaussian envelope. From these results, we conclude that the higher-order Stern-Gerlach effect can be generalized to the fully higher-order Poincaré-sphere spinors with nontrivial topological structures.

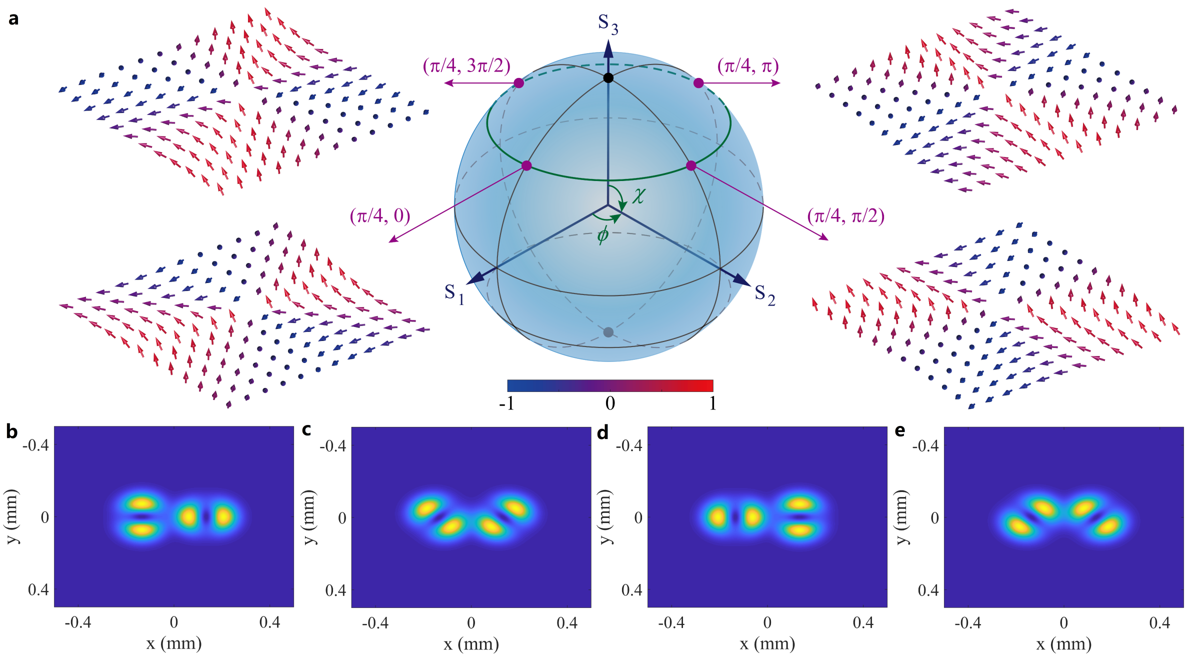

FIG. S4: **The higher-order Stern-Gerlach effect for the off-equator spin textures.** **a**, The spin textures located at (χ, ϕ)= ($\pi/4$, 0), (χ, ϕ)= ($\pi/4$, $\pi/2$), (χ, ϕ)= ($\pi/4$, π) and (χ, ϕ)= ($\pi/4$, $3\pi/2$) of the first-order (ℓ=1) Poincaré sphere. **b-e**, The splittings of these spin textures in the presence of the synthetic magnetic field gradient ($U = 600$ V). **b**, $\varphi = 0$, **c**, $\varphi = \pi/2$, **d**, $\varphi = \pi$, and **e**, $\varphi = 3\pi/2$.